A&A manuscript no.
(will be inserted by hand later)

Your thesaurus codes are:
07 (08.09.2; 08.01.1; 08.01.3; 08.05.3; 08.23.1)

ASTRONOMY
AND
ASTROPHYSICS
16.5.1996

Spectral analysis of the hot DO white dwarf PG 1034+001*

K. Werner[1], **S. Dreizler**[2] **and B. Wolff**[1]

[1] Institut für Astronomie und Astrophysik der Universität Kiel, D-24098 Kiel, Federal Republic of Germany
[2] Dr.-Remeis-Sternwarte, Universität Erlangen-Nürnberg, Sternwartstr. 7, D-96049 Bamberg, Federal Republic of Germany

Received date; accepted date

Abstract. We present a non-LTE model atmosphere analysis of the hot DO white dwarf PG 1034+001. It is based on archival HST GHRS spectra, on new optical medium resolution spectra and pointed ROSAT PSPC observations.

The effective temperature is higher than previously thought ($T_{\rm eff}$=100 000 K, $\log g$ =7.5). We determined abundances of carbon, nitrogen, and oxygen which are roughly in agreement with earlier LTE results. We also determined the silicon abundance and, for the first time in a DO white dwarf, the abundance of iron on hand of newly identified Fe VI lines in the HST spectra. An upper abundance limit for nickel is derived. The results are discussed in the framework of diffusion theory.

We derive a stellar mass of 0.59 $M_\odot$ and propose that PG 1034+001 is a descendant from the hydrogen-deficient PG 1159 stars.

Key words: stars: individual: PG 1034+001– stars: abundances – stars: atmospheres – stars: evolution – white dwarfs

1. Introduction

PG 1034+001 is a helium rich, hot white dwarf which was spectroscopically classified as a "hot DO" star (Wesemael et al. 1985, henceforth WGL). From low resolution optical and ultraviolet (IUE) spectrophotometry using LTE model atmospheres WGL estimated the effective temperature and surface gravity as to $T_{\rm eff}$=80 000±20 000 K and $\log g > 7$. With V=13.23 (Landolt 1992) PG 1034+001 is the brightest hot DO and therefore best suited for high resolution spectroscopic studies in order to determine the atmospheric parameters and metal abundances. The results are important to test the theory of element diffusion in white dwarfs, which predicts that specific species may be kept from gravitational settling by radiative acceleration.

Consequently, a high resolution IUE spectrum obtained with the SWP camera was used by Sion et al. (1985, SLW) to identify spectral lines and to determine the photospheric abundances of carbon, nitrogen, and oxygen by means of a LTE analysis of the line equivalent widths, adopting $T_{\rm eff}$=80 000 K and $\log g$ =8. These abundances, in particular the seven times solar abundance of nitrogen, were interpreted in terms of selective radiative forces acting in the high-temperature photosphere. Poulin et al. (1989) have argued that PG 1034+001 is probably hotter than 80 000 K, based on an examination of the absolute continuum flux distribution including Voyager observations.

In the present work we extend the analysis of PG 1034+001 to include medium resolution high-S/N optical spectra, high resolution UV spectra (Hubble Space Telescope data) retrieved from the archive, and X-ray data obtained with ROSAT. The superior quality of the new observational data (presented in Sect. 2) allows a more precise determination of the parameters and element abundances, and will be used to analyse for the first time the silicon and iron abundance in PG 1034+001 (Sect. 3). Non-LTE model atmospheres and line formation calculations, appropriate for the high temperature encountered, will be used. Our conclusions are presented in Sect. 4.

2. Observations

2.1. Optical spectra

A medium resolution (about 3.5Å) spectrum was taken in January 1992 with the 3.5m New Technology Telescope of the ESO at La Silla (exposure time: 45 min). Attached was the ESO Multi Mode Instrument, which was used with a dichroic that splits the light beyond the slit into a blue and a red beam, feeding two separate spectroscopic channels. We employed the CCDs ESO#18 (THX31156, 19μ, 1024^{2}px) and ESO#28 (TX1024m, 24μ, 1024^{2}px), gratings #12 (39Å/mm) and #7 (56Å/mm). The slit width corresponds to 1.2 arcsec on the sky. The useful portion of the spectrum covers the wavelengths 4250–4800Å and 5700–6700Å.

Send offprint requests to: K. Werner

* Based on observations obtained a) at the European Southern Observatory, La Silla, Chile; b) at the German-Spanish Astronomical Center, Calar Alto, operated by the Max-Planck-Institut für Astronomie Heidelberg jointly with the Spanish National Commission for Astronomy; c) with the ROSAT, HST, IUE, and EXOSAT satellites. This research has made use of the Simbad database, operated at CDS, Strasbourg, France

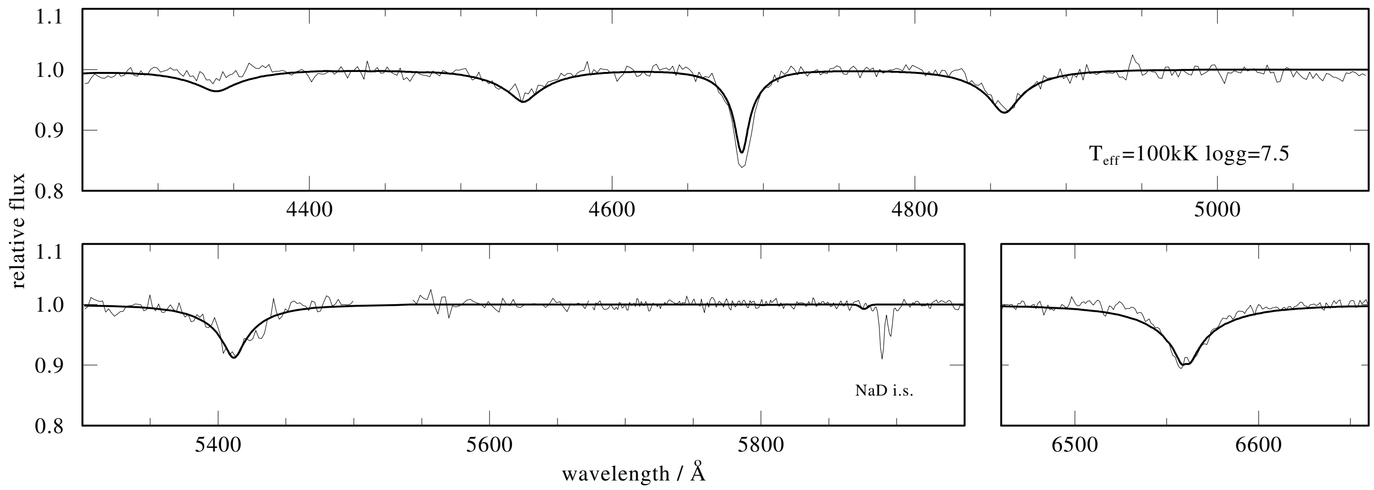

Fig. 1. Normalized optical spectrum of PG 1034+001. Bluewards of 5670Å: Calar Alto data (resolution 6Å), else: NTT data (resolution 3.5Å). Overplotted are synthetic spectra folded with Gaussians with respective FWHMs, from a model with the adopted atmospheric parameters

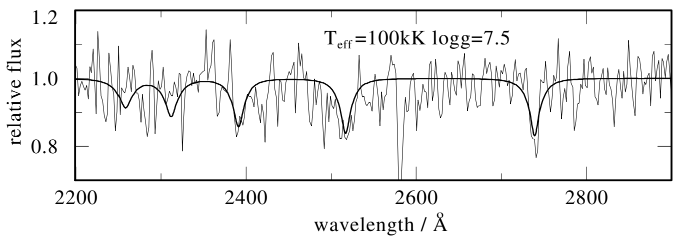

Fig. 2. IUE LWR and synthetic spectrum (folded with a 5Å FWHM Gaussian) from the final model

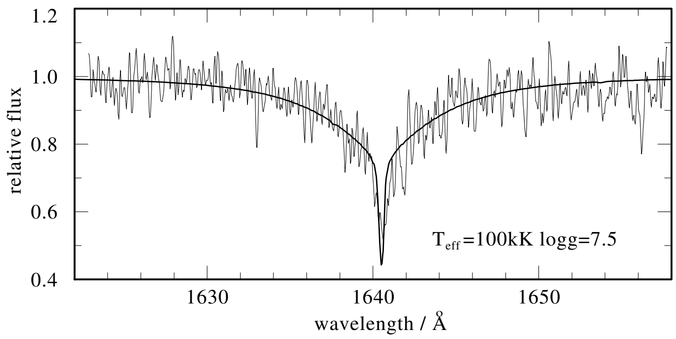

Fig. 3. HST spectrum showing the He II 1640 line (smoothed with a Gaussian with 0.1Å FWHM) and synthetic spectrum from the final model

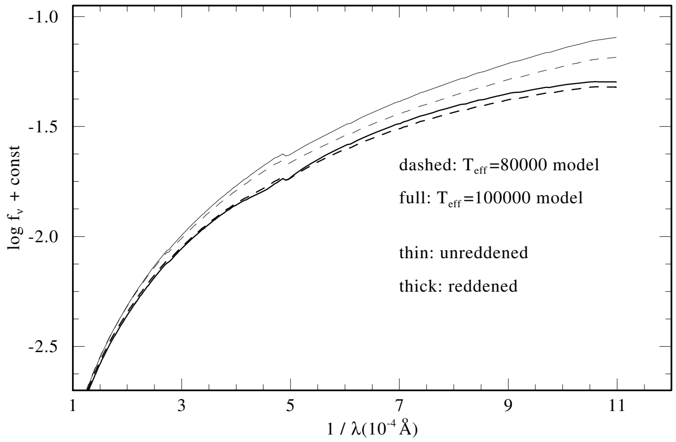

Fig. 4. Continuum fluxes of two models with different $T_{\rm eff}$ from the optical region down to the Lyman limit, normalized to fit in the V band (thin lines). Also shown are the same models affected by interstellar reddening in slightly different amounts: E(B-V)=0.02 and 0.03 for the 80 000 K and 100 000 K models, respectively. Both models are almost indistinguishable if the reddening is not known accurately enough

This spectrum is complemented by a low resolution (about 6Å) spectrum taken in November 1990 with 3.5m telescope on Calar Alto (Spain) and kindly provided by Stefan Jordan (exposure time: 17 min). The TWIN spectrograph, which also works with a dichroic, was used, along with two gratings (144Å/mm and 160Å/mm) and two CCDs (RCA, 15μ, 1024 × 640 px; and GEC, 22μ, 1155 × 768 px) for the blue and red channels, respectively. The slit width was 1.76 arcsec. The spectrum covers the range between 3500Å and 7000Å. All images were wavelength calibrated with He-Ar comparison spectra and flat-fielded with dome-flats.

No stellar features but He II absorption lines appear in the optical spectra (Fig. 1). In particular we do not see He I.

2.2. Ultraviolet HST and IUE spectra

Five high resolution UV spectra obtained with the Goddard High Resolution Spectrograph (GHRS) of the Hubble Space Telescope (HST) in June 1992 were retrieved from the archive. Each of them covers a wavelength interval of approximately 35Å; some details were presented by Shipman et al. (1993). Exposure times amount to 288 sec except for the spectrum around the N V resonance line which was exposed for 576 sec. The G160M grating was used which gives a resolving power of 20 000 or a resolution of about 0.06-0.08Å. The following stellar absorption lines are identified: The N V, C IV, and Si IV resonance doublets, He II 1640Å, and O V 1371Å. A few Fe VI/VII

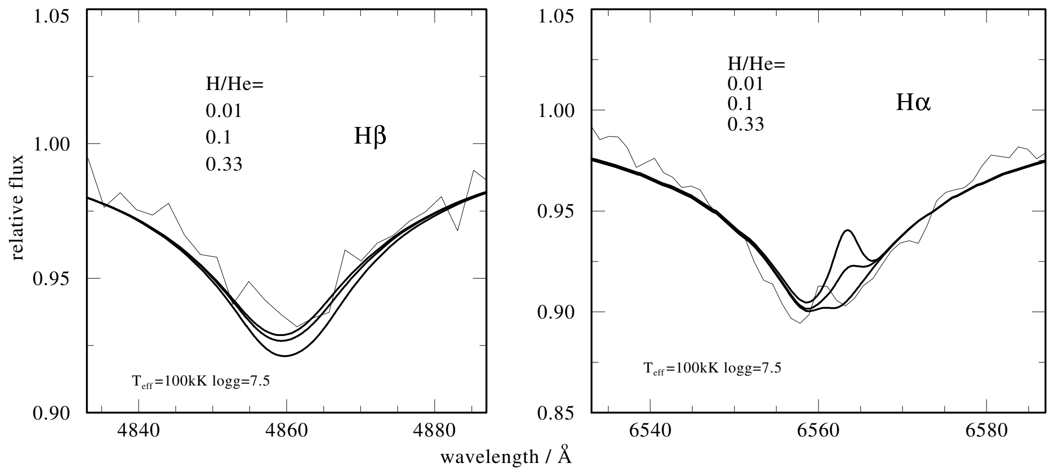

Fig. 5. Determination of the upper limit for the hydrogen abundance. The Hβ line core becomes deeper with increasing H/He ratio. In contrary, Hα developes an emission core. We adopt H/He$<$10%

lines can be detected (see Tab. 1). All resonance lines exhibit stellar and interstellar contributions as was already pointed out by SLW based on IUE observations. Many other interstellar absorption lines of neutral or singly ionized species are detectable including a strong hydrogen Ly α line.

A high resolution IUE spectrum taken with the SWP camera (image number SWP 18509) was examined in detail by SLW and Fritz et al. (1990, FLS). They showed that the absorption lines are divided into two groups. One of it has a radial velocity around 0 km/sec and can be attributed to interstellar or circumstellar material. The other group is red-shifted by about 40 km/sec and is of photospheric origin: The He II 1640Å and O V 1371Å lines and blends of C IV 1550Å, N V 1240Å, and Si IV near 1400Å with their interstellar counterparts. Somewhat surprising the Si IV line was declared as "conspicuous by its absence" by SLW in the IUE spectrum although it appears to be present quite securely. This was also noted later by FLS who claim the presence of this line based on another IUE echelle spectrum (SWP 26201).

The question as to the origin of the non-photospheric lines has been speculated about by other authors. Yet, the present data do not allow to decide between circumstellar or interstellar material. The former hypothesis might support the idea of past or on-going mass-loss from PG 1034+001 as discussed by FLS. But these authors found no evidence for this idea in a detailed study. However, they considered the possibility of real line profile changes, but this is not conclusive from the present data. Noteable asymmetries in some lines, like the O V 1371Å and N V 1240Å were attributed to the possible presence of circumstellar material or mass-loss. In the case of O V the asymmetry is due to a blend with a previously unidentified Fe VI line. In the case of N V this is simply due to a interstellar contribution to the blue absorption line wings, which is resolved by the HST data, and not a signature of mass-loss as argued by SLW.

We have measured the radial velocities of all lines identified in the HST spectra and the result is shown in Tab. 1. The new observations qualitatively confirm the finding by SLW and the velocities fall into one of two distinct groups separated by about 50 km/sec. However, a comparison with their table 1 reveals that all lines which appear in both (IUE and HST) datasets have systematically different measured wavelengths. The HST velocities are more blue by about 15 km/sec on the average, corresponding to about 0.08Å. This value is just below the IUE resolution and just above the HST resolution, which could explain the systematic difference. Somwhat disturbing is the velocity of the red component of the Si IV line. This is possibly due to the fact that the interstellar and stellar components are strongly blended and difficult to measure (see Fig. 8). The detection of the iron features is new, except for the Fe VII 1240Å line which was originally discovered by Feibelman & Bruhweiler (1990).

A low resolution IUE spectrum taken with the LWR camera (LWR 09888) was retrieved from the archive. It was already used by WGL to identify the just detectable He II lines of the Fowler series. This spectrum will be used below to check if our final model is consistent with the observation.

2.3. X-ray data

We have performed two pointed observations of PG 1034+001 with the X-ray satellite ROSAT. Total exposure times were 11163 sec (in May 1992) and 18111 sec (in June 1993). The source was detected by the X-ray telescope with the PSPC (Position Sensitive Proportional Counter) but not with the Wide Field Camera. The photons were extracted and reduced with the EXSAS software package (Version 1993, Zimmermann et al. 1993). The count rates were corrected for dead time and vignetting. An EXOSAT observation from 1984 (Paerels & Heise 1989) is used as an additional consistency check for the final model.

3. Determination of atmospheric parameters

Non-LTE model atmospheres were constructed using the ALI (Accelerated Lambda Iteration) code of Werner (1986). They are composed mainly of helium but also include hydrogen and carbon although the latter two species are trace elements and

Table 1. PG 1034+001 UV line identifications in the HST spectra. Colons indicate less certain measurements

Ion	$\lambda_{\rm obs}$(Å)	$\lambda_{\rm rest}$(Å)	Shift (km s^{-1})
He II	1640.62	1640.43	+35
C IV	1548.11	1548.19	-15:
	1548.37	1548.19	+35
	1550.70	1550.77	-14
	1550.93	1550.77	+31
N I	1199.43	1199.55	-30
	1200.13	1200.22	-22
	1200.61	1200.71	-25
N V	1238.74	1238.81	-17
	1238.93	1238.81	+29
	1242.74	1242.80	-14
	1242.92	1242.80	+29
O V	1371.44	1371.29	+33
Si II	1190.31	1190.42	-28
	1193.20	1193.29	-23
Si III	1206.42	1206.51	-22
Si IV	1393.66	1393.76	-22
	1393.91	1393.76	+32
	1402.78	1402.77	-2 :
	1403.00	1402.77	+50:
S II	1250.49	1250.59	-24
	1253.67	1253.81	-33:
Fe VI	1228.65	1228.61	+10:
	1230.09	1229.95	+34
	1232.57	1232.48	+22
	1240.21	1240.07	+34
	1252.90	1252.79	+26
	1253.75	1253.67	+20:
	1370.88	1370.73	+33
	1371.21	1371.07	+31
	1374.77	1374.63	+31
Fe VII	1208.52	1208.37	+37
	1239.78	1239.69	+22
	1244.62	1244.44	+43
	1251.94	1251.86	+19

do not affect the line profile fits described in the following. Using temperature and density stratification of these models, subsequent line formation iterations were performed for Si, N, and O. For computational details and atomic data used, see Werner et al. (1994) and references therein.

For the determination of the iron abundance and for the analysis of the ROSAT data as well, line blanketed model atmospheres including H, He, C, N, O and the iron group elements (solar relative abundances among the latter) self-consistently were used. For details on these models see Dreizler & Werner (1993). Similar models for the estimation of the nickel abundance were introduced by Werner & Dreizler (1994). An important improvement concerns the introduction of bound-free photon cross-sections for iron from the Opacity Project (Seaton et al. 1994) data base (TOPBASE, CDS Strasbourg, Cunto & Mendoza 1992), which strongly affect the EUV fluxes.

3.1. Effective temperature and surface gravity

The optical He II line profiles were used to determine $T_{\rm eff}$ and $\log g$. Figure 1 shows the normalized observed spectra together with synthetic spectra from the model that was found to fit the data best. This model has $T_{\rm eff}$=100 000 K and $\log g$ =7.5. Obviously the fit is not as satisfying as one might wish, in particular, the He II 4340Å line is not as shallow as in the observation. A higher $\log g$ would help here but this may be excluded from the fact that He I 5876Å is not observed. Both, increasing $\log g$ by 0.5 dex or decreasing $T_{\rm eff}$ by 10 000 K causes it to show up as a weak absorption line in the models. On the other hand, increasing $T_{\rm eff}$ by more than 15 000 K requires decreasing $\log g$ by 0.5 dex in order to keep the depth of the line cores in the other He II lines. Lowering $\log g$ by 0.3 dex would help to fit better the He II 6560Å line but then the discrepancy at 4340Å becomes drastic. In spite of these uncertainties +15kK/-10kK for $T_{\rm eff}$ and 0.3 dex for $\log g$ are regarded as reasonable errors.

As stated in previous analyses (Werner et al. 1994), He II 4686Å may not be fitted at all and the reason for this failure is still unknown. SLW have taken a high resolution (0.2Å) spectrum of this line and it shows a sharp emission reversal. This reversal is not visible in our data which have a much lower resolution. Our final model does show this emission, however, it is too weak when compared to the observation by SLW. We have demonstrated this discrepancy already in our analysis of the hot DO KPD 0005+5106 and we have attributed the sharp (and much stronger, compared to PG 1034+001) emission core to a possible temperature inversion in the upper atmosphere layers below the suspected corona. In the case of PG 1034+001 there are no signs of a corona in the X-ray data so another explanation must be looked for. Interestingly, Madej (1994) has claimed that Compton heating can cause a temperature rise in the outer layers of hot white dwarf (LTE) atmospheres. This could cause the 4686Å emission reversal in PG 1034+001 (and also in KPD 0005+5106). We have not yet tested this alternative explanation because the generalization of the Compton heating formalism to NLTE conditions is not a trivial task.

Clearly, near UV spectra of the He II Fowler series would be useful to find tighter limits for temperature and gravity. PG 1034+001 has been observed by IUE with the LWR camera, but the spectra are too noisy. Figure 2 shows the normalized spectrum of image LWR 09888 together with a computed spectrum from our $T_{\rm eff}$=100 000 K/logg=7.5 model. Three lines can be identified and at least they do not contradict our results from the optical observations.

Instead, the He II 1640Å line covered by one of the HST spectra may be utilized as a consistency check. Figure 3 shows the spectrum together, again, with our favoured $T_{\rm eff}$=100 000 K/logg=7.5 model. The fit is almost perfect, aside from the innermost line core which is slightly too deep in the model profile.

In principle it is possible to determine $T_{\rm eff}$ from the continuous flux distribution. But it is well known that this method is rather insensitive at the temperatures in question here, because the optical and IUE spectral ranges cover the Rayleigh-Jeans

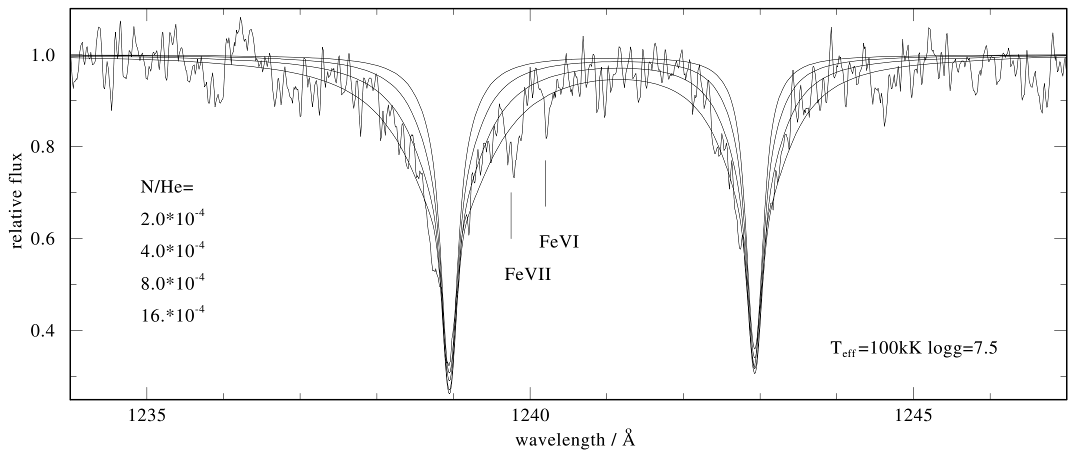

Fig. 6. Determination of the nitrogen abundance from the N V resonance line in the HST GHRS spectrum (not smoothed). We adopt N/He= $6 \cdot 10^{-4}$

tail of the stellar flux. Poulin et al. (1989) have tried to escape this limitation and extended the observed spectral range closer to the stellar flux maximum on hand of a Voyager spectrum (900Å-1200Å) together with optical broad band and IUE low resolution data. From the fact that the overall fit of a 80 000 K model is quite satisfactory except of the Voyager region (where the flux was underestimated by their model) they concluded that $T_{\rm eff}$ is probably higher than 80 000 K. But they could not give a more quantitative result realizing that the difficulties encountered with the interstellar reddening are hard to overcome. In fact, we have made a test calculation which shows that the flux distributions of a 80 000 K model and a 100 000 K model are almost indistiguishable when one applies only slightly different reddening values: E(B-V)=0.02 (the value determined by WGL) to the cooler and E(B-V)=0.03 (favoured by Poulin et al.) to the hotter model gives almost the same results (see Fig. 4). Interestingly, even the 100 000 K model underestimates the flux observed by Voyager unless one reduces the reddening to an unrealistically low value. This might be a hint that the absolute flux calibration of the Voyager spectrum gives too large fluxes. Aside from the calibration problem we conclude that this method is unreliable to constrain $T_{\rm eff}$ of PG 1034+001.

3.2. Trace element abundances: H, C, N, O, Si, Fe, Ni

The above determined basic parameters $T_{\rm eff}$ and $\log g$ are kept fixed during the following considerations concerning the abundance determinations of trace elements. However, these parameters were varied within their estimated error ranges in order to investigate the influence on the quantities derived and to establish error limits.

First of all we are interested in the amount of hydrogen which might still be present in the atmosphere without showing up as distortions in the corresponding He II absorption lines. Figure 5 shows a close-up of the He II lines at the position of Hβ and Hα. Overplotted are three profiles computed from models with different H/He number ratios: 1%, 10%, and 33%. Although the 4860Å profile is best approached by the model with 1% hydrogen (which is identical to a pure helium pro-

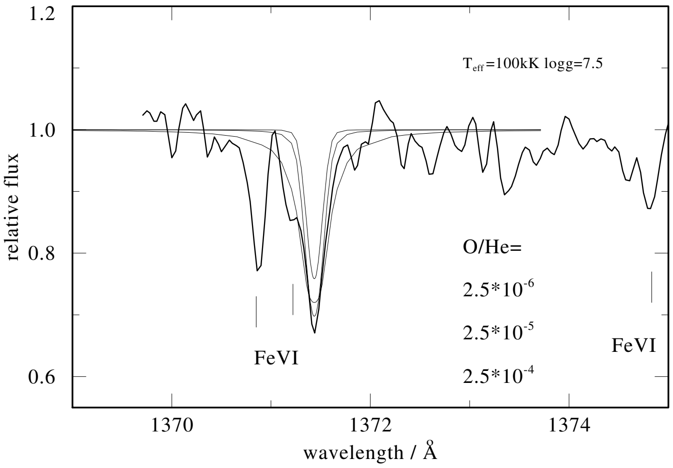

Fig. 7. Determination of the oxygen abundance from the O V 1371Å line in the HST GHRS spectrum (smoothed with a 0.1Å FWHM Gaussian). We adopt O/He= $8 \cdot 10^{-5}$ Note also three newly identified Fe VI lines

file), the additional depression of the line core due to hydrogen opacity is uncomfortably small, even in the 33% model. More sensitive to hydrogen traces is the He II line at Hα. Although we have mentioned problems to fit the line wings, the line core is matched well by the model with 1% (or less) hydrogen. The presence of H by about 10% causes the development of a central emission reversal, which is conspicuous in the 33% profile. We adopt H/He=10% as an upper limit for the hydrogen abundance in PG 1034+001. This Hα emission is well known from hot DAs (Reid & Wegner 1989) and is a typical NLTE effect. The emission might be strengthened by mechanisms like discussed above for the He II 4686Å line. As Δn=1 transitions these lines are particularly susceptible to the development of emission cores. In any case, such a strengthening would make Hα detectable at an even lower abundance so that our upper limit becomes even more conservative.

The nitrogen abundance is determined from a fit to the N V resonance doublet at 1240Å. A detail of the HST spectrum is shown in Fig. 6 together with four synthetic profiles. They

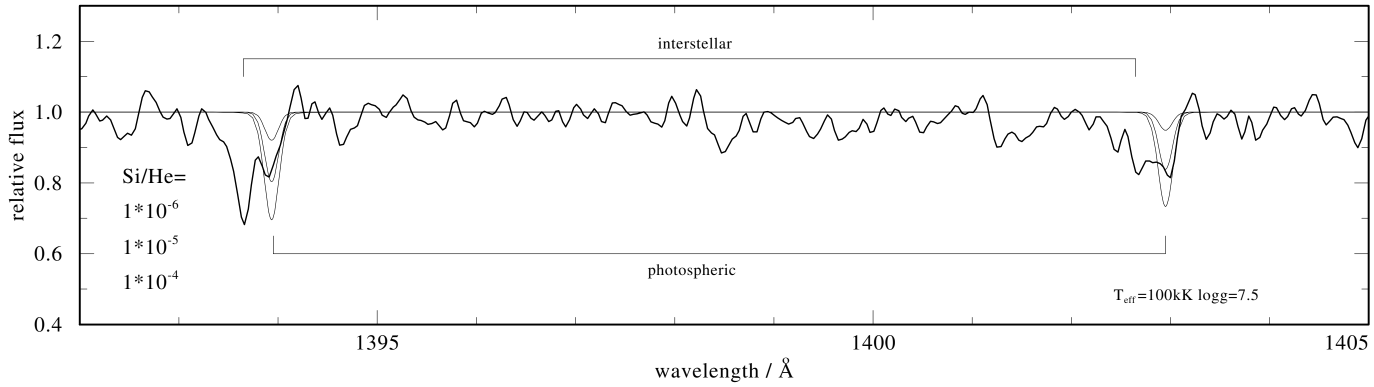

Fig. 8. Determination of the silicon abundance from the Si IV doublet in the HST GHRS spectrum (smoothed with a 0.1Å FWHM Gaussian). We adopt Si/He= 10^{-5}

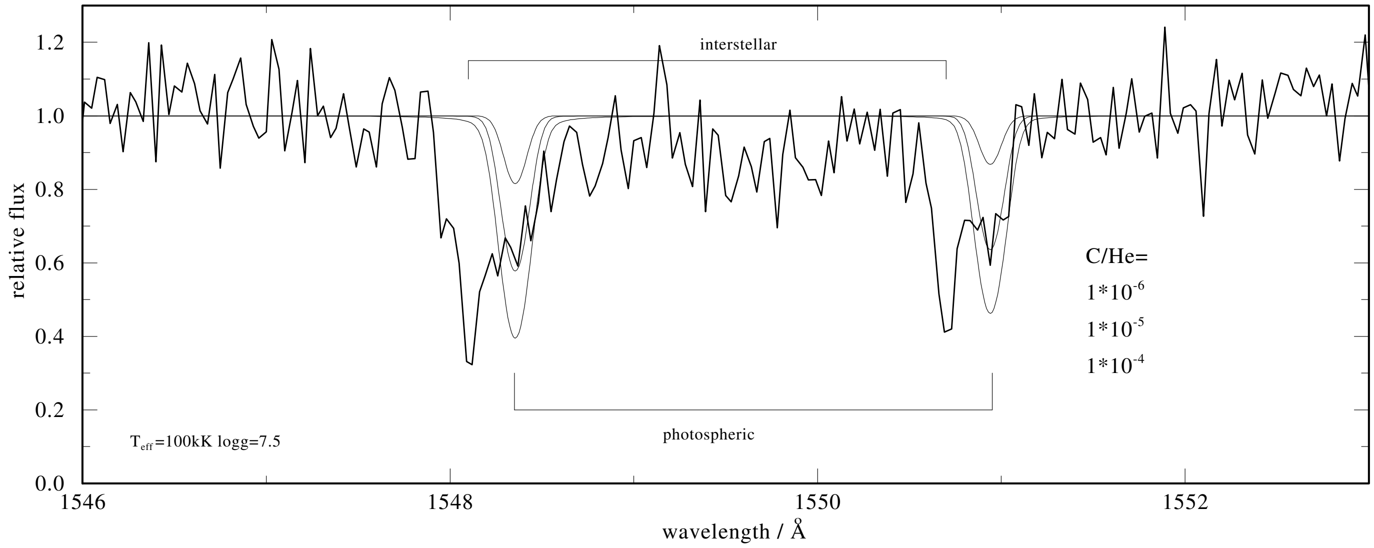

Fig. 9. Determination of the carbon abundance from the C IV resonance doublet in the HST GHRS spectrum (not smoothed). We adopt C/He= 10^{-5}

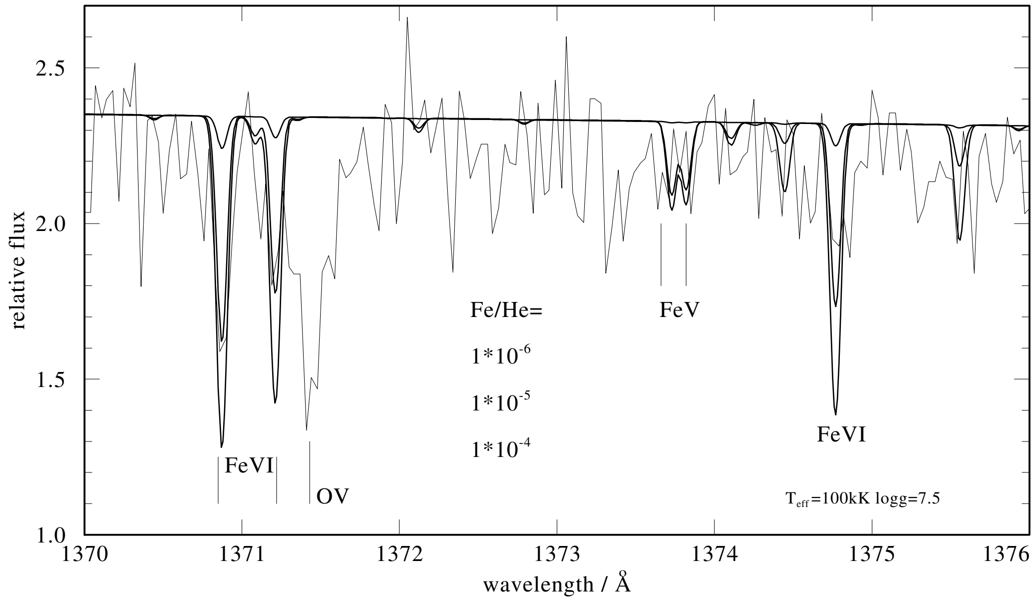

Fig. 10. Determination of the iron abundance from Fe VI lines in the HST GHRS spectrum near O V 1371Å (not smoothed). The synthetic spectra show iron lines, only. We adopt Fe/He= 10^{-5}: The model profiles for the two Fe VI lines near 1371Å almost coincide with the observation

are from models with N/He number ratios of 2, 4, 8, and $16 \cdot 10^{-4}$. The best fit is achieved between N/He=4 and $8 \cdot 10^{-4}$, i.e. log(N/He)=-3.2, and the error is estimated to ± 0.3 dex. The doublet is blended by very weak interstellar N v components, which are visible as blueshifted (relative to the photospheric components) absorptions close to the line cores. As indicated in Fig. 6 we note the presence of two iron lines (Fe vi and Fe vii) in between the N v doublet.

The O v 1371Å line is covered by one of the HST spectra. It is the only means to find the oxygen abundance. However, the spectrum is rather noisy so that we must accept quite large possible errors. In addition this line is very temperature sensitive so that the uncertainty in the $T_{\rm eff}$ determination makes the abundance estimate even less reliable. Fig. 7 shows that O/He=$2.5 \cdot 10^{-6}$ is clearly too weak to match the observed line profile. It appears that the observation requires O/He somewhere between $2.5 \cdot 10^{-4}$ and $2.5 \cdot 10^{-5}$. We adopt log(O/He)=-4.1 ± 0.5. We note another absorption feature, which is blueward of the O v line by about 0.5Å. It may be attributed to photospheric iron (see below).

The Si iv doublet near 1400Å shows an interstellar and a photospheric component (Fig. 8). We present three synthetic profiles, which are from models with log(Si/He)= $-4, -5, -6$. The photospheric silicon abundance amounts to log(Si/He)= -5 ± 0.3 dex.

Similarly, the C iv resonance doublet near 1550Å shows a strong interstellar component and a weaker photospheric line (Fig. 9). Three computed line profiles are shown, from which we deduce a carbon abundance of log(C/He)=-5 ± 0.3 dex.

The iron abundance is determined from three Fe vi lines in the vicinity of O v 1371Å (Fig. 10). We computed three models, with log(Fe/He)= $-4, -5, -6$. We derive log(Fe/He)= -5 ± 0.3 dex. We failed to fit the Fe vii line near 1240Å with any of the models computed. In contrast a good fit was obtained in the case of the hot (hydrogen-rich) subdwarf BD+28 4211 (Dreizler & Werner 1993). The failure here is currently analysed.

An upper limit for the nickel abundance is estimated from Fig. 11. It covers the wavelength region of the GHRS spectra at hand where we do expect the two strongest lines (Ni vi). It is obvious that the S/N of the observation does not allow an identification of the lines and we conclude that log(Ni/He)< -5.

In summary, we derived the following atmospheric parameters for PG 1034+001:

$T_{\rm eff}$=100 000 K $^{+15\,000}_{-10\,000}$
log g =7.5 $\pm$ 0.3 (cgs units)
log(H/He)≤ -1.0 (number ratio)

The metal abundances are given in Tab. 2.

Let us compare our derived CNO abundances with the result of the previous LTE analysis by SLW. They have found log(C/He)=-5.5, log(N/He)=-3.1, log(O/He)=-3.6 with somewhat larger error limits than ours. Thus, within error limits, the NLTE and LTE results agree. Does this mean that the LTE abundance determination for hot DOs is reliable? It is not the intention of this paper to make a systematic study comparing LTE and NLTE models. Instead we show on hand of a single example that the close agreement of the results in the case of PG 1034+001 might be coincidental and may not be generalized to other species.

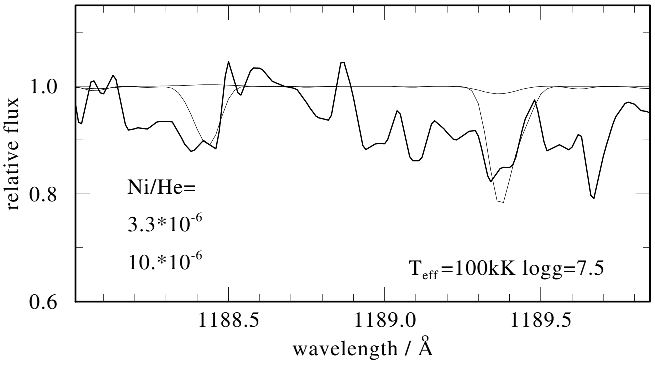

Fig. 11. Estimation of an upper limit for the nickel abundance from calculated Ni vi lines in comparison with the HST GHRS spectrum (smoothed with a 0.1Å FWHM Gaussian). We adopt Ni/He$< 10^{-5}$

Table 2. Observed metal abundances in the hot DO white dwarfs PG 1034+001 and KPD 0005+5106 and predictions from diffusion theory (Chayer et al. 1994a)

	PG 1034+001		KPD 0005+5106	
	$T_{\rm eff}$=100 000 K log g =7.5		$T_{\rm eff}$=120 000 K log g =7	
	observed	predicted	observed	predicted
log C/He	-5.0 ± 0.3	-3.7	-3.5 ± 0.5	-3.7
log N/He	-3.2 ± 0.3	-3.1	-4.0 ± 0.5	-3.1
log O/He	-4.1 ± 0.5	-2.8	< -4.0	-2.3
log Si/He	-5.0 ± 0.3	-5.9		
log Fe/He	-5.0 ± 0.3	-3.3		
log Ni/He	< -5.0			

Fig. 12 shows a comparison between the LTE and NLTE line profile of the O v 1371Å line. The LTE line core is much deeper because of an overionization of O v in the NLTE model as compared to the LTE model. A similar effect was found by Dreizler & Werner (1993) for Fe v lines in the extreme UV range of hot DAs. If we reduce $T_{\rm eff}$ of the model from 100 000 K to 80 000 K then the change of the profile is of the order of the LTE-NLTE difference. Thus, the 0.5 dex difference between our analysis of the O abundance and that of SLW partially reflects the NLTE effects. It is dangerous to generalize this numerical value to other species because NLTE effects are unpredictable. Thus they should be taken into account for hot DO model atmosphere analyses.

3.3. Interpretation of the X-ray data

Our metal line blanketed model atmospheres were used to compute synthetic ROSAT PSPC pulse height distributions taking into account interstellar absorption. Details of this procedure are described in Jordan et al. (1994a). A calibration factor of 2 was applied to the theoretical distribution, following the analyses of hot DA white dwarfs by Napiwotzki et al. (1993) and Jordan et al. (1994b).

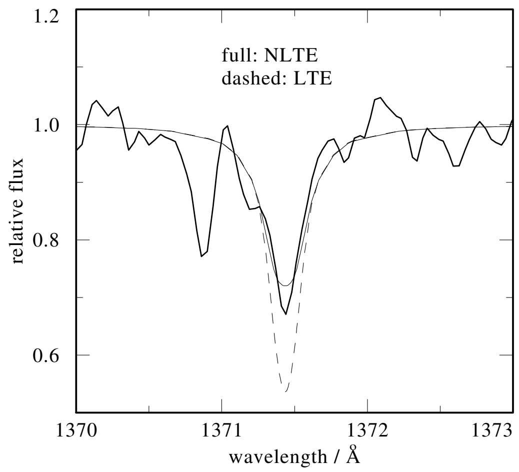

Fig. 12. Comparison of a LTE and a NLTE line profile to the observation. The model parameters are: $T_{\rm eff}$=100 000 K, log g =7.5, log(O/He)=−3.6.

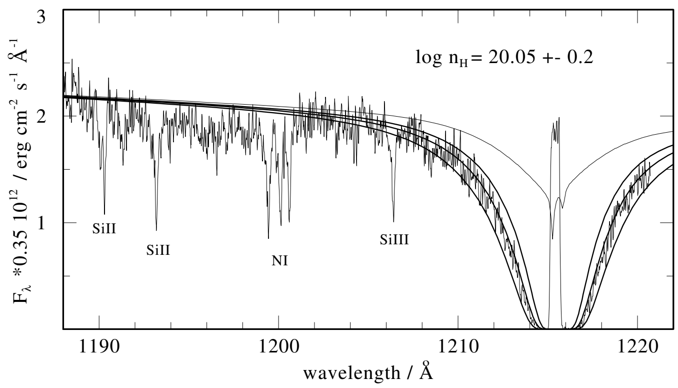

Fig. 13. Determination of the interstellar hydrogen column density from Lyman α in the HST GHRS spectrum. The central emission is of geocoronal origin. We show the photospheric He II profile (plus contribution of 1% hydrogen; from model $T_{\rm eff}$=100 000 K, log g =7.5) and the same profile after interstellar absorption with 3 different values for the column density (log $n_{\rm H}$ = 20.05 ± 0.2)

Models with $T_{\rm eff}$=100kK and lower could be excluded from the outset because their flux beyond the He II ground state edge is much too low. Instead we used models with $T_{\rm eff}$=110kK, a value still within the error limits determined from the analysis above. All other atmospheric parameters were kept fixed to the values found above, with the exception of the iron abundance. Iron turns out to be the most important EUV opacity source and was therefore adjusted to achieve a fit to the observations. The interstellar hydrogen column density derived from the Lyman α profile in the HST spectrum (log $n_{\rm H}$ = 20.05 ± 0.2, see Fig. 13) is an important constraint for the fitting procedure. It should be noted that the contribution of the photospheric He II line to the Lyman α feature is not entirely negligible here and was taken into account. The neglect of He II would give a H column density higher by 0.2 dex.

Figure 14 shows two results. The dashed line is the synthetic spectrum from the model which has abundances equal or close to those which were finally accepted from the UV line

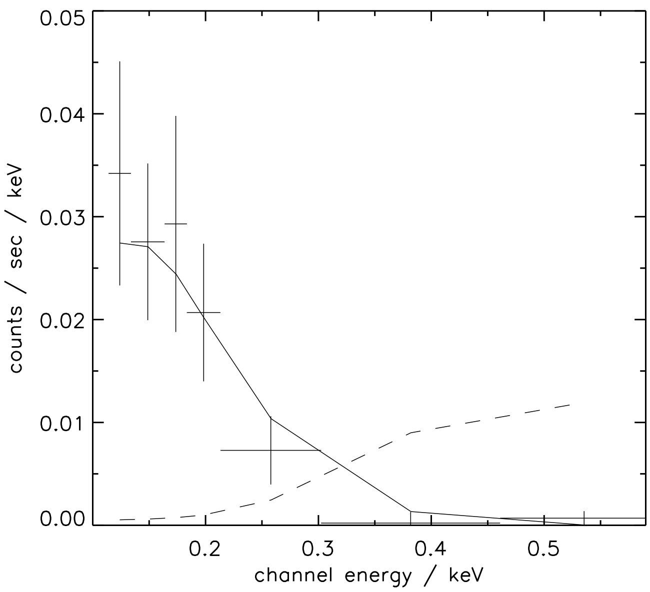

Fig. 14. Comparison of the ROSAT pulse height spectrum of PG 1034+001 (crosses indicate 1σ errors) with the predicted count rate for two iron line blanketed NLTE models with $T_{\rm eff}$=110 000 K and log g =7.5. Dashed line: log(Fe/He)= -5, log $n_{\rm H}$ = 21.3. Full line: log(Fe/He)= -4, log $n_{\rm H}$ = 20.2. The interstellar hydrogen column density was adjusted to fit the total count rate. Only the model with the high EUV opacity provided by iron bound-free transitions gives a satisfying fit with an $n_{\rm H}$ that is consistent with the value derived from Lyman α

data (log(C/He)= -5.5, log(N/He)= -3.1, log(O/He), = -3.6, log(Fe/He)= -5). In order to conserve the total count rate, an unrealistically high interstellar column density is required (log $n_{\rm H}$ = 21.3). Additionally the spectrum is much too hard, being a consequence of a flux increase in the model beyond 200eV. Obviously, the EUV opacity is too weak in this case. We therefore increased the iron abundance by a factor of 10 and then a satisfactory fit is found together with a interstellar column density (log $n_{\rm H}$ = 20.2) which is in accordance with the Lyman α profile.

This iron abundance is a factor of 3 too high, even if we allow for a value at the edge of the error limit of the UV analysis. The reason for this discrepancy is unclear but a reasonable explanation might be the neglect of inner shell ionization cross sections in the iron atomic data from the Opacity Project (Pradhan priv. comm.). Alternatively the missing opacity could come from other iron group elements. Their abundances might be enhanced well above the solar value without being notable in the UV region (see our considerations above about nickel). But present computing capacities do not allow to compute various abundance patterns among the iron group. In addition no bound-free photon cross-sections for iron group elements other than iron itself are available. Nevertheless, the ROSAT data serve as an additional constraint for the effective temperature determination.

We have taken the model which fits the ROSAT data best, folded it with the EXOSAT instrument response and compared the predicted count rates with observations published by Paerels & Heise (1989). PG 1034+001 was only detected in the 3LX/LE1 filter with 0.0017–0.0072 counts/sec (99% confidence level) which agrees well with our prediction: 0.0021 counts/sec. PG 1034+001 was not detected in the AlP/LE1 filter which means that the count rate is <0.0068. In fact our model predicts a count rate more than a factor of 10 below this upper observational limit. Similarly, the non-detection of PG 1034+001 by the ROSAT Wide Field Camera through filters S1a and P2 is consistent with our predictions.

4. Discussion and conclusions

Comparing the position of PG 1034+001 in the $\log g$ –$\log T_{\rm eff}$ diagram with theoretical evolutionary tracks (Fig. 15) gives the stellar mass and luminosity:

$$M/M_{\odot} = 0.59^{+.14}_{-.03}$$
$$\log L/L_{\odot} = 1.9^{+.5}_{-.5}$$

The distance of PG 1034+001 is determined from its surface gravity and angular diameter. The latter is derived by comparison of the measured visual flux (V=13.23, the low interstellar extinction is neglected) to the model flux (parameters: $T_{\rm eff}$=100 000 K, $\log g$ =7.5, H/He/C = 1/100/.01 number ratios; H_{ν}[5400Å] = $1.3 \cdot 10^{-3}$ erg cm^{-2} s^{-1} Hz^{-1}):

$$d\ [\mathrm{pc}] = 155^{+58}_{-43}$$

corresponding to a height of 115^{+43}_{-32} pc above the galactic plane.

From the position of PG 1034+001 in the $\log g$ –$\log T_{\rm eff}$ diagram we conclude that the hot DO star is probably a descendant from the PG 1159 stars. For a detailed discussion and alternative evolutionary scenarios see the considerations in Werner et al. (1994) for the slightly hotter DO star KPD 0005+5106 which also apply here.

If we accept the hypothesis that the metal abundances in KPD 0005+5106 are determined by the interplay of gravitational settling and radiative levitation then this is also certainly the case in PG 1034+001 because it is more evolved. In Tab. 2 we compare the observed metal abundances in both DOs to the predictions from latest diffusion theory calculations (Chayer et al. 1994a). It can be seen that some agreement is achieved, however, in many cases the predictions cannot reproduce the observations (e.g. in the cases of iron and carbon). At the present state of diffusion calculations such a comparison is certainly premature and needs to be repeated after the improvement of theory as was pointed out by Chayer et al. (1994b). Such calculations still lack the potential presence of other mechanisms which may interfere and compete with radiative levitation and gravitational settling such as weak stellar winds and blocking effects of different metals among each other.

Acknowledgements. We thank an anonymous referee for his constructive criticism which helped to improve the paper. We are grateful to Pierre Chayer for passing to us the results of his diffusion calculations prior to publication. K.W. was supported by the BMFT and DFG (grants 50 OR 9302 4 and We 1312/6-1) and S.D. by the DFG under grant He 1356/16-1. A DFG travel grant to the Calar Alto observatory is acknowledged. Computations were carried out on CRAY computers in Kiel, Erlangen, and Munich.

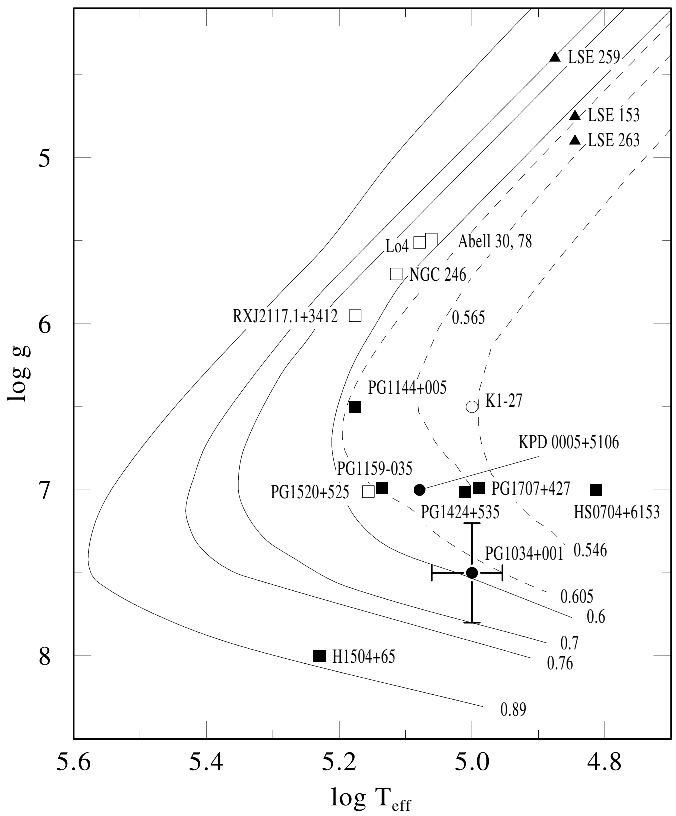

Fig. 15. Position of PG 1034+001 in the $\log g$ –$\log T_{\rm eff}$ diagram. Open symbols: associated PN, full symbols: no associated PN. Circles: He-dominated objects, squares: He-C-dominated objects (i.e. PG 1159 stars), triangles: He-rich sdO stars. Evolutionary tracks are labeled with the respective stellar mass (in solar units). Dashed: H burners (Schönberner 1983; Blöcker & Schönberner 1990), solid: He burners (Wood & Faulkner 1986)

References

Blöcker T., Schönberner D. 1990, A&A 240, L11
Chayer P., Fontaine G., Wesemael F. 1994a, in preparation
Chayer P., LeBlanc F., Fontaine G., et al. 1994b, ApJ submitted
Cunto W., Mendoza C. 1992, Rev. Mexicana Astron. Af. 23, 107
Dreizler S., Werner K. 1993, A&A 278, 199
Feibelman W.A., Bruhweiler F.C. 1990, ApJ 357, 548
Fritz M.L., Leckenby H.J., Sion E.M. 1990, AJ 99, 908 (FLS)
Jordan S., Mürset U., Werner K. 1994a, A&A 283, 475
Jordan S., Wolff B., Koester D., Napiwotzki R. 1994b, A&A in press
Landolt A.U. 1992, AJ 104, 340
Madej J. 1994, A&A 286, 515
Napiwotzki R., Barstow M.A., Fleming T. et al. 1993, A&A 278, 478
Paerels F.B.S., Heise J. 1989, ApJ 339, 1000
Poulin E., Wesemael F., Holberg J.B., Fontaine G. 1989, in White Dwarfs, IAU Coll. 114, ed. G.Wegner, Lecture Notes in Physics, Springer-Verlag, Berlin, p. 144
Reid N., Wegner G. 1989, in White Dwarfs, IAU Coll. 114, ed. G.Wegner, Lecture Notes in Physics, Springer-Verlag, Berlin, p. 396

Seaton M.J., Yan Y., Mihalas D., Pradhan A.K. 1994, MNRAS 266, 805
Schönberner D. 1983, ApJ 272, 708
Shipman H.L., Barnhill M., Bond H. et al. 1993, in White Dwarfs: Advances in Observation and Theory, ed. M.A.Barstow, NATO ASI Series C, Vol. 403, Kluwer, Dordrecht, p. 67
Sion E.M., Liebert J., Wesemael F. 1985, ApJ 292, 477 (SLW)
Werner K. 1986, A&A 161, 177
Werner K., Dreizler S. 1994, A&A 286, L31
Werner K., Heber U., Fleming T.A. 1994, A&A 284, 907
Wesemael F., Green R.F., Liebert J. 1985, ApJS 58, 379 (WGL)
Wood P.R., Faulkner D.J. 1986, ApJ 307, 659
Zimmermann H.U., Belloni T., Izzo C. et al. 1993, EXSAS User's Guide, MPE Report 244

This article was processed by the author using Springer-Verlag LaTeX A&A style file *L-AA* version 3.